# Effects of $p$-$d$ hybridization on the valence band of I-III-$VI_2$ chalcopyrite semiconductors

Kajornyod Yoodee* and John C. Woolley
*Physics Department, University of Ottawa, Ottawa, Ontario, Canada K1N 6N5*

Virulh Sa-yakanit
*Physics Department, Chulalongkorn University, Bangkok 10500, Thailand*
(Received 15 June 1984)

The electronic structure of the valence band at the Brillouin-zone center of the I-III-$VI_2$ chalcopyrite compounds has been calculated using a model developed by adding the effects of $p$-$d$ hybridization and the crystal field to the Hamiltonian of the Kane model. Two important parameters in the model are the energy separation $E$ between the $p$ and $d$ levels and the interaction $M$ between these levels. It is shown that three previous models (Tell and Bridenbaugh, Kildal, and the linear hybridization model) can be derived as special cases of the present model. The model has been used to analyze the available data on some 13 compounds. It is shown that the dimensionless parameters $M/E$ and $\Delta E_g/E$, where $\Delta E_g$ is the band-gap anomaly, show a smooth variation with the fractional $d$ character of the valence band and appear to be characteristic of the structure. Values of the deformation potentials $b_p$ and $b_d$ averaged over all of the compounds have been determined and found to be $b_p=(-0.8\pm0.2)$ eV and $b_d=(-4.3\pm1.5)$ eV.

## I. GENERAL INTRODUCTION

Considerable interest has been shown in recent years[1-3] in the chalcopyrite compounds and their alloys because of their possible technological applications, e.g., in solar-energy conversion, potential utilization in light-emitting diodes, nonlinear-optical materials, etc. Earlier studies have shown that the structure of the uppermost valence bands in a II-IV-$V_2$ chalcopyrite compound is simply related to the energy bands of its III-V binary analog. It has also been found that the Hopfield quasicubic model[4] can be used to satisfactorily explain the observed splitting and symmetry properties of the valence bands at the Brillouin-zone center. The $s$-like conduction band is nondegenerate (doubly degenerate counting spins) and the $p$-like valence band is triply degenerate (sixfold degenerate with spins). The triple degeneracy of the $p$-like valence bands which are derived from the $\Gamma_{15}$ level in the zinc-blende structure is completely removed by the simultaneous effects of the spin-orbit and crystal-field interactions. The largest contribution to the crystal-field splitting of the valence bands comes from the noncubic potential arising from the tetragonal lattice compression along the chalcopyrite $z$ axis.[1]

Kildal[5] generalized the Kane theory[6] of energy-band structure near $\vec{k}=\vec{0}$ to the ternary chalcopyrite compounds by including in the Hamiltonian a $k$-independent crystal-potential anisotropy, adjusted to reproduce the experimentally observed valence-band splitting at $\vec{k}=\vec{0}$. Within this model, the energies of the $\Gamma_7$ levels relative to $\Gamma_6(E_0=0)$ level in the valence bands are given by

$$E_{1,2}=-\tfrac{1}{2}(\Delta+\delta)\pm\tfrac{1}{2}[(\Delta+\delta)^2-\tfrac{8}{3}\Delta\delta]^{1/2}\,, \qquad (1)$$

which is exactly the same form as that of Hopfields's quasicubic model. The crystal-field-splitting, $\delta$, and spin-orbit-splitting, $\Delta$, parameters can thus be determined from the observed valence-band-splitting data using Eq. (1). This theory can be satisfactorily applied to the II-IV-$V_2$ compounds.

In the case of I-III-$VI_2$ compounds, the uppermost valence bands are profoundly influenced by the proximity of noble-metal $d$ levels, as has been pointed out by Shay and Wernick[1] and by Jaffe and Zunger.[7] Two manifestations of the hybridization of anion $p$ levels and noble-metal $d$ levels have been observed. The direct energy gaps observed in I-III-$VI_2$ compounds are smaller than the energy gaps in the II-VI analogs by amounts of up to 2.41 eV (in the case of $CuAlS_2$), and the spin-orbit splittings are considerably smaller than those of II-VI analogs.[3] The strong $p$-$d$ hybridization of the valence bands has been directly determined from the x-ray-photoemission studies.[8] The compounds containing Cu show a stronger $p$-$d$ hybridization effect than the Ag compounds.

Tell and Bridenbaugh[9] proposed a simple model, which takes into account the $p$-$d$ hybridization of the valence bands at the center of the Brillouin zone of a quasicubic crystal. Two important parameters are the energy separation $E$ between the $p$- and $d$-like $\Gamma_{15}$ levels and the interaction matrix element $M$ between these levels. The basis of the model is that two levels of the same symmetry will mix and repel each other, the magnitude of the interaction depending on the energy separation and the strength of the interaction potential. In the model, it was assumed that the $\Gamma_{15}$ levels of the $p$ and $d$ bands in the absence of $p$-$d$ hybridization would be midway between the corresponding $\Gamma_8$ and $\Gamma_7$ levels. This, however, is not the case.[6] In addition, the effect of the crystal field was not taken into account. According to the results of Tell and Bridenbaugh, to explain the effect of the negative spin-orbit splitting in $CuGaS_2$, the unperturbed $d$-like $\Gamma_{15}$ level must lie above the unperturbed $p$-like $\Gamma_{15}$ level.

 

## II. THEORY

### A. Introduction

Here, a model is proposed which takes into account the $p$-$d$ hybridization effect on the uppermost valence bands of I-III-$VI_2$ chalcopyrite compounds, considering only the center of the Brillouin zone (BZ). For convenience, it is assumed that the $p$-like valence bands lie above the $d$-like ones, although a similar analysis could be carried out without this assumption. In a cubic (tetrahedral) field, the fivefold-degenerate $d$ levels split into a threefold-degenerate $\Gamma_{15}(d)$ and a twofold-degenerate $\Gamma_{12}(d)$ set, and it can be shown that the $\Gamma_{15}(d)$ levels lie at higher energy than the $\Gamma_{12}(d)$. The $d$ level $\Gamma_{15}(d)$ has the same symmetry as the $p$ level $\Gamma_{15}(p)$, so that these will interact with each other. Since the $d$ level $\Gamma_{12}(d)$ has the wrong symmetry to interact with the $\Gamma_{15}(p)$, it can be neglected. Thus only the $p$ band $\Gamma_{15}(p)$ and the $d$ band $\Gamma_{15}(d)$ will be considered.

There are two important parameters in this model, viz., the energy separation $E$ between $p$ and $d$ levels and the interaction matrix element $M$ due to the $p$-$d$—hybridization interaction between these levels. Starting from a quasicubic crystal with spin-orbit interaction, the wave functions of the diagonalized spin-orbit interaction are used as basis functions. The $p$-$d$—hybridization interaction is applied and levels of the same symmetry will mix and repel each other, the magnitude of the interaction depending on the energy separation and the strength of the interaction potential. The interaction is responsible for both the reduction $\Delta E_g$ in the energy gap compared with the value for the corresponding binary compound (i.e., the band-gap anomaly) and for the reduced or negative spin-orbit splitting.

In order to see the effect of the crystal field on the uppermost valence bands, the first three mixed levels, which have $\Gamma_8$ and $\Gamma_7$ symmetry, are then perturbed further, and they split into three separate levels with $\Gamma_7$, $\Gamma_6$, and $\Gamma_7$ symmetry, respectively. All of the energy eigenvalues and wave functions, including the coefficient of $d$-like character, can then be determined exactly. The two parameters $E$ and $M$ will later be treated as adjustable parameters so as to fit the energy eigenvalues to the experimental data. The parameters $E$, $M$, and the band-gap anomaly $\Delta E_g$ play an important role in the theory. Three special cases will be considered, viz., the cases when there is no $p$-$d$ hybridization and/or crystal field, and the one when the strength of the interaction potential is very weak.

### B. Theoretical development

The Hamiltonian for cubic crystals with spin-orbit interaction is of the form

$$H=\frac{p^2}{2m}+V_0+\frac{\hbar}{4m^2c^2}(\vec{\nabla}V_0\times\vec{\mathrm{p}})\cdot\vec{\sigma}\ , \tag{2}$$

where $\vec{\mathrm{p}}$ is the momentum operator and $\vec{\sigma}$ is the spin operator. The term $V_0$ is the cubic potential of the crystal.

The basis functions in the diagonalized spin-orbit Hamiltonian can be written as follows:[6] For the $p$ band,

$$\phi^{\alpha}_{p1}(\Gamma_8)=(\tfrac{1}{3})^{1/2}\left|\frac{X-iY}{\sqrt{2}}\uparrow\right\rangle+(\tfrac{2}{3})^{1/2}|Z\downarrow\rangle\ ,$$

$$\phi^{\alpha}_{p0}(\Gamma_8)=\left|\frac{X+iY}{\sqrt{2}}\uparrow\right\rangle \tag{3}$$

$$\phi^{\alpha}_{p2}(\Gamma_7)=(\tfrac{2}{3})^{1/2}\left|\frac{X-iY}{\sqrt{2}}\uparrow\right\rangle-(\tfrac{1}{3})^{1/2}|Z\downarrow\rangle\ ,$$

$$\phi^{\beta}_{p1}(\Gamma_8)=(\tfrac{1}{3})^{1/2}\left|-\frac{X+iY}{\sqrt{2}}\downarrow\right\rangle+(\tfrac{2}{3})^{1/2}|Z\uparrow\rangle\ ,$$

$$\phi^{\beta}_{p0}(\Gamma_8)=\left|\frac{X-iY}{\sqrt{2}}\downarrow\right\rangle\ , \tag{4}$$

$$\phi^{\beta}_{p2}(\Gamma_7)=(\tfrac{2}{3})^{1/2}\left|-\frac{X+iY}{\sqrt{2}}\downarrow\right\rangle-(\tfrac{1}{3})^{1/2}|Z\uparrow\rangle\ .$$

The first three functions are degenerate, respectively, with the last three. For the $d$ band,

$$\phi^{\alpha}_{d1}(\Gamma_8)=(\tfrac{1}{3})^{1/2}\left|\frac{YZ-iZX}{\sqrt{2}}\uparrow\right\rangle+(\tfrac{2}{3})^{1/2}|XY\downarrow\rangle\ ,$$

$$\phi^{\alpha}_{d0}(\Gamma_8)=\left|\frac{YZ+iZX}{\sqrt{2}}\uparrow\right\rangle\ , \tag{5}$$

$$\phi^{\alpha}_{d2}(\Gamma_7)=(\tfrac{2}{3})^{1/2}\left|\frac{YZ-iZX}{\sqrt{2}}\uparrow\right\rangle-(\tfrac{1}{3})^{1/2}|XY\downarrow\rangle\ ,$$

$$\phi^{\beta}_{d1}(\Gamma_8)=(\tfrac{1}{3})^{1/2}\left|-\frac{YZ+iZX}{\sqrt{2}}\downarrow\right\rangle+(\tfrac{2}{3})^{1/2}|XY\uparrow\rangle\ ,$$

$$\phi^{\beta}_{d0}(\Gamma_8)=\left|\frac{YZ-iZX}{\sqrt{2}}\downarrow\right\rangle\ , \tag{6}$$

$$\phi^{\beta}_{d2}(\Gamma_7)=(\tfrac{2}{3})^{1/2}\left|-\frac{YZ+iZX}{\sqrt{2}}\downarrow\right\rangle-(\tfrac{1}{3})^{1/2}|XY\uparrow\rangle\ .$$

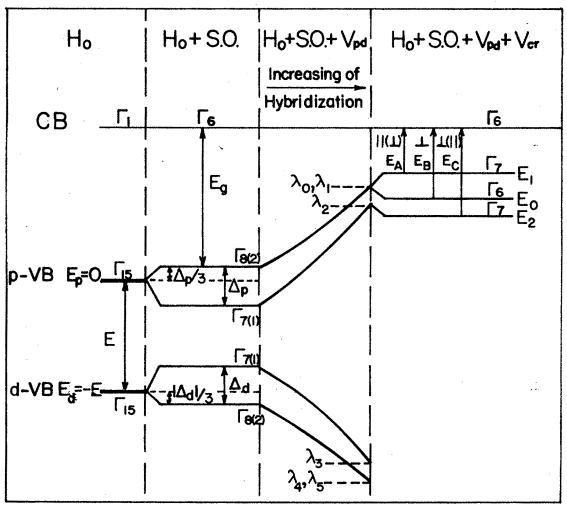


FIG. 1. Sketch of the energy-band configuration at the Γ point showing the variations in the $p$ and $d$ bands as spin-orbit interaction, $p$-$d$ hybridization, and crystal-field interaction are successively applied.

The first three of these functions are again degenerate, respectively, with the last three.

These are the wave functions which form a set of orthonormalized states for the noninteracting $p$ and $d$ bands. The resulting energy configuration is shown in Fig. 1.

In the presence of a hybridization interaction potential $V_{pd}$, the interaction matrix can be written as

$$\begin{bmatrix} \mathscr{V}_{pd} & 0 \\ 0 & \mathscr{V}_{pd} \end{bmatrix} . \tag{7}$$

The basis wave functions used in this representation are as follows: $\phi^{\alpha}_{p1}(\Gamma_8)$, $\phi^{\alpha}_{d1}(\Gamma_8)$, $\phi^{\alpha}_{p0}(\Gamma_8)$, $\phi^{\alpha}_{d0}(\Gamma_8)$, $\phi^{\alpha}_{p2}(\Gamma_7)$, $\phi^{\alpha}_{d2}(\Gamma_7)$, $\phi^{\beta}_{p1}(\Gamma_8)$, $\phi^{\beta}_{d1}(\Gamma_8)$, $\phi^{\beta}_{p0}(\Gamma_8)$, $\phi^{\beta}_{d0}(\Gamma_8)$, $\phi^{\beta}_{p2}(\Gamma_7)$, and $\phi^{\beta}_{d2}(\Gamma_7)$. The first six functions are degenerate with the last six, respectively. The matrix elements and the submatrix $\mathscr{V}_{pd}$ can be written in the form

$$\begin{aligned} &\langle \phi^{\alpha}_{pi}(\Gamma_m) \mid V_{pd} \mid \phi^{\beta}_{dj}(\Gamma_n) \rangle = M\delta_{ij}\delta_{\alpha\beta}\delta_{mn} , \\ &\langle \phi^{\alpha}_{pi}(\Gamma_m) \mid V_{pd} \mid \phi^{\beta}_{pj}(\Gamma_n) \rangle = 0 , \\ &\langle \phi^{\alpha}_{di}(\Gamma_m) \mid V_{pd} \mid \phi^{\beta}_{dj}(\Gamma_n) \rangle = 0 , \end{aligned} \tag{8}$$

where $M$ is the interaction between these levels and $\delta_{ij}$ is a Kronecker $\delta$ function. The full matrix representation then becomes

$$\mathscr{V}_{pd} = \begin{bmatrix} \Delta_p/3 & M & 0 & 0 & 0 & 0 \\ M & -E-|\Delta_d|/3 & 0 & 0 & 0 & 0 \\ 0 & 0 & \Delta_p/3 & M & 0 & 0 \\ 0 & 0 & M & -E-|\Delta_d|/3 & 0 & 0 \\ 0 & 0 & 0 & 0 & -\frac{2}{3}\Delta_p & M \\ 0 & 0 & 0 & 0 & M & -E+\frac{2}{3}|\Delta_d| \end{bmatrix} , \tag{9}$$

where $\Delta_p$ and $\Delta_d$ are the spin-orbit splitting of the $p$ and $d$ band, respectively. The resulting energy eigenvalues are

$$\lambda_0=\lambda_1=\frac{1}{2}\left[\frac{\Delta_p}{3}-E-\frac{|\Delta_d|}{3}\right]+\frac{1}{2}\left[\left[\frac{\Delta_p}{3}+E+\frac{|\Delta_d|}{3}\right]^2+4M^2\right]^{1/2} ,$$

$$\lambda_2=\tfrac{1}{2}(-\tfrac{2}{3}\Delta_p-E+\tfrac{2}{3}|\Delta_d|)+\tfrac{1}{2}[(-\tfrac{2}{3}\Delta_p+E-\tfrac{2}{3}|\Delta_d|)^2+4M^2]^{1/2} , \tag{10}$$

$$\lambda_3=\tfrac{1}{2}(-\tfrac{2}{3}\Delta_p-E+\tfrac{2}{3}|\Delta_d|)-\tfrac{1}{2}[(-\tfrac{2}{3}\Delta_p+E-\tfrac{2}{3}|\Delta_d|)^2+4M^2]^{1/2} ,$$

$$\lambda_4=\lambda_5=\frac{1}{2}\left[\frac{\Delta_p}{3}-E-\frac{|\Delta_d|}{3}\right]-\frac{1}{2}\left[\left[\frac{\Delta_p}{3}+E+\frac{|\Delta_d|}{3}\right]^2+4M^2\right]^{1/2} , \tag{11}$$

and the corresponding eigenfunctions are as follows: for $\lambda_0$,

$$\begin{aligned} &\Phi^{\alpha}_0(\Gamma_8)=a_0\phi^{\alpha}_{p0}(\Gamma_8)+b_0\phi^{\alpha}_{d0}(\Gamma_8) , \\ &\Phi^{\beta}_0(\Gamma_8)=a_0\phi^{\beta}_{p0}(\Gamma_8)+b_0\phi^{\beta}_{d0}(\Gamma_8) , \end{aligned} \tag{12}$$

for $\lambda_1$,

$$\begin{aligned} &\Phi^{\alpha}_1(\Gamma_8)=a_1\phi^{\alpha}_{p1}(\Gamma_8)+b_1\phi^{\alpha}_{d1}(\Gamma_8) , \\ &\Phi^{\beta}_1(\Gamma_8)=a_1\phi^{\beta}_{p1}(\Gamma_8)+b_1\phi^{\beta}_{d1}(\Gamma_8) , \end{aligned} \tag{13}$$

for $\lambda_2$,

$$\begin{aligned} &\Phi^{\alpha}_2(\Gamma_7)=a_2\phi^{\alpha}_{p2}(\Gamma_7)+b_2\phi^{\alpha}_{d2}(\Gamma_7) , \\ &\Phi^{\beta}_2(\Gamma_7)=a_2\phi^{\beta}_{p2}(\Gamma_7)+b_2\phi^{\beta}_{d2}(\Gamma_7) , \end{aligned} \tag{14}$$

for $\lambda_3$,

$$\begin{aligned} &\Phi^{\alpha}_3(\Gamma_7)=a_3\phi^{\alpha}_{p2}(\Gamma_7)+b_3\phi^{\alpha}_{d2}(\Gamma_7) , \\ &\Phi^{\beta}_3(\Gamma_7)=a_3\phi^{\beta}_{p2}(\Gamma_7)+b_3\phi^{\beta}_{d2}(\Gamma_7) , \end{aligned} \tag{15}$$

for $\lambda_4$,

$$\begin{aligned} &\Phi^{\alpha}_4(\Gamma_8)=a_4\phi^{\alpha}_{p0}(\Gamma_8)+b_4\phi^{\alpha}_{d0}(\Gamma_8) , \\ &\Phi^{\beta}_4(\Gamma_8)=a_4\phi^{\beta}_{p0}(\Gamma_8)+b_4\phi^{\beta}_{d0}(\Gamma_8) , \end{aligned} \tag{16}$$

and for $\lambda_5$,

$$\begin{aligned} &\Phi^{\alpha}_5(\Gamma_8)=a_5\phi^{\alpha}_{p1}(\Gamma_8)+b_5\phi^{\alpha}_{d1}(\Gamma_8) , \\ &\Phi^{\beta}_5(\Gamma_8)=a_5\phi^{\beta}_{p1}(\Gamma_8)+b_5\phi^{\beta}_{d1}(\Gamma_8) . \end{aligned} \tag{17}$$

The $a_i$ and $b_i$ coefficients can be evaluated. Writing $\gamma_i=a_i^2$, then

$$\gamma_0=\gamma_1=a_1^2=1-b_1^2 = 1\Big/\left[1+M^2\Big/\left[\lambda_1+E+\frac{|\Delta_d|}{3}\right]^2\right] , \tag{18}$$

$$\gamma_2=a_2^2=1-b_2^2=1/[1+M^2/(\lambda_2+E-\tfrac{2}{3}|\Delta_d|)^2] , \tag{19}$$

$$\gamma_3=a_3^2=1-b_3^2=1-1/[1+M^2/(\lambda_3+\tfrac{2}{3}\Delta_p)^2] , \tag{20}$$

$$\gamma_4=\gamma_5=a_5^2=1-b_5^2=1-1\Big/\left[1+M^2\Big/\left[\lambda_5-\frac{\Delta_p}{3}\right]^2\right] . \tag{21}$$

Next, it is necessary to include the crystal-field interaction due to the noncubic potential arising from the tetragonal lattice compression along the chalcopyrite $z$ axis, this being the largest contribution to the crystal-field splitting of the valence bands. In order to find the splitting of the uppermost valence bands, only the first three levels are considered. Using the wave-function equations (12)—(14) as basis functions, the interaction matrix for the crystal-field interaction, $V_{\rm cr}$, can be written as

$$\begin{vmatrix} \lambda_1-\gamma_1\frac{\delta_p}{3}-(1-\gamma_1)\frac{\delta_d}{3} & (2\gamma_1\gamma_2)^{1/2}\frac{\delta_p}{3}+[2(1-\gamma_1)(1-\gamma_2)]^{1/2}\frac{\delta_d}{3} & 0 \\ (2\gamma_1\gamma_2)^{1/2}\frac{\delta_p}{3}+[2(1-\gamma_1)(1-\gamma_2)]^{1/2}\frac{\delta_d}{3} & \lambda_2 & 0 \\ 0 & 0 & \lambda_0+\gamma_0\frac{\delta_p}{3}+(1-\gamma_0)\frac{\delta_d}{3} \end{vmatrix} . \tag{22}$$

The quantities $\delta_p$ and $\delta_d$ are the crystal-field-splitting parameters of the $p$ and $d$ bands, respectively. They are defined by[5]

$$\langle X \mid V_{\rm cr} \mid X\rangle=\langle Y \mid V_{\rm cr} \mid Y\rangle=\frac{\delta_p}{3} , \tag{23}$$

$$\langle Z \mid V_{\rm cr} \mid Z\rangle=-\tfrac{2}{3}\delta_p , \tag{24}$$

and, similarly,

$$\langle YZ \mid V_{\rm cr} \mid YZ\rangle=\langle ZX \mid V_{\rm cr} \mid ZX\rangle=\frac{\delta_d}{3} , \tag{25}$$

$$\langle XY \mid V_{\rm cr} \mid XY\rangle=-\tfrac{2}{3}\delta_d . \tag{26}$$

It is to be noted that the static shift[5] due to the crystal field has already been taken into account. However, the cross-term matrix element due to the crystal field has been neglected in the present model.

To determine the level splittings at the BZ center, the matrix in Eq. (22) must be diagonalized. The valence band then splits into three doubly degenerate levels, which are

$$E_0(\Gamma_6)=\lambda_0+\gamma_0\frac{\delta_p}{3}+(1-\gamma_0)\frac{\delta_d}{3} , \tag{27}$$

$$E_{1,2}(\Gamma_7)=\frac{1}{2}\left[\lambda_1+\lambda_2-\gamma_1\frac{\delta_p}{3}-(1-\gamma_1)\frac{\delta_d}{3}\right] \pm\frac{1}{2}\left[\left[\lambda_1-\lambda_2-\gamma_1\frac{\delta_p}{3}-(1-\gamma_1)\frac{\delta_d}{3}\right]^2+\tfrac{8}{9}\{(\gamma_1\gamma_2)^{1/2}\delta_p+[(1-\gamma_1)(1-\gamma_2)]^{1/2}\delta_d\}^2\right]^{1/2} . \tag{28}$$

In order to estimate a value for the band-gap anomaly $\Delta E_g$, it is assumed that the $\Gamma_8$ level in this analysis is the same as the top level in the valence band of the equivalent binary compound. In that case, $\Delta E_g$ then takes the value

$$\Delta E_g=E_1-\Delta_p/3 . \tag{29}$$

The wave functions corresponding to Eqs. (27) and (28) are

$$\Psi_1^\alpha(\Gamma_7)=c_1\Phi_1^\alpha(\Gamma_8)+d_1\Phi_2^\alpha(\Gamma_7)=c_1a_1\phi_{p1}^\alpha(\Gamma_8)+d_1a_2\phi_{p2}^\alpha(\Gamma_7)+c_1b_1\phi_{d1}^\alpha(\Gamma_8)+d_1b_2\phi_{d2}^\alpha(\Gamma_7) , \tag{30}$$

$$\Psi_1^\beta(\Gamma_7)=c_1a_1\phi_{p1}^\beta(\Gamma_8)+d_1a_2\phi_{p2}^\beta(\Gamma_7)+c_1b_1\phi_{d1}^\beta(\Gamma_8)+d_1b_2\phi_{d2}^\beta(\Gamma_7) , \tag{31}$$

$$\Psi_0^\alpha(\Gamma_6)=\Phi_0^\alpha(\Gamma_8)=a_0\phi_{p0}^\alpha(\Gamma_8)+b_0\phi_{do}^\alpha(\Gamma_8) , \tag{32}$$

$$\Psi_0^\beta(\Gamma_6)=\Phi_0^\beta(\Gamma_8)=a_0\phi_{p0}^\beta(\Gamma_8)+b_0\phi_{d0}^\beta(\Gamma_8) , \tag{33}$$

and

$$\Psi_2^\alpha(\Gamma_7)=c_2\Phi_1^\alpha(\Gamma_8)+d_2\Phi_2^\alpha(\Gamma_7)=c_2a_1\phi_{p1}^\alpha(\Gamma_8)+d_2a_2\phi_{p2}^\alpha(\Gamma_7)+c_2b_1\phi_{d1}^\alpha(\Gamma_8)+d_2b_2\phi_{d2}^\alpha(\Gamma_7) , \tag{34}$$

$$\Psi_2^\beta(\Gamma_7)=c_2a_1\phi_{p1}^\beta(\Gamma_8)+d_2a_2\phi_{p2}^\beta(\Gamma_7)+c_2b_1\phi_{d1}^\beta(\Gamma_8)+d_2b_2\phi_{d2}^\beta(\Gamma_7) . \tag{35}$$

Using these levels, the fractional $p$-like character of the uppermost valence bands are found to be

$$\alpha_1=c_1^2a_1^2+d_1^2a_2^2=c_1^2\gamma_1+d_1^2\gamma_2 , \tag{36}$$

$$\alpha_0=a_0^2=\gamma_0 , \tag{37}$$

and

$$\alpha_2=c_2^2a_1^2+d_2^2a_2^2=c_2^2\gamma_1+d_2^2\gamma_2\ , \tag{38}$$

where

$$c_1^2=1\Big/\left[1+\left[(2\gamma_1\gamma_2)^{1/2}\frac{\delta_p}{3}+[2(1-\gamma_1)(1-\gamma_2)]^{1/2}\frac{\delta_d}{3}\right]^2\Big/(E_1-\lambda_2)^2\right]\ , \tag{39}$$

$$d_2^2=1\Big/\left[1+\left[(2\gamma_1\gamma_2)^{1/2}\frac{\delta_p}{3}+[2(1-\gamma_1)(1-\gamma_2)]^{1/2}\frac{\delta_d}{3}\right]^2\Big/\left[E_2-\lambda_1+\gamma_1\frac{\delta_p}{3}+(1-\gamma_1)\frac{\delta_d}{3}\right]^2\right]\ , \tag{40}$$

$$c_1^2+d_1^2=1\ , \tag{41}$$

$$c_2^2+d_2^2=1\ . \tag{42}$$

Thus, from the above analysis, the energy separations of the valence bands are given by Eqs. (27) and (28), and the fractional $p$ and $d$ characters of the valence are given by Eqs. (36)—(38). Equations (27) and (28) can be used to analyze the experimental data available for various chalcopyrite materials and give values for the various material parameters. This will be done in Sec. IV. Before this analysis, however, it is instructive to show that the present model will reduce to the previously proposed models under the appropriate limits.

## III. LIMITING CASES

Three previous models are considered and it is shown that each is a special case of the present model and can be derived from it.

### A. Tell and Bridenbaugh model

In the Tell and Bridenbaugh analysis, there is no noncubic crystal field and, in the absence of $p$-$d$ hybridization, the $\Gamma_{15}$ levels of the $p$ and $d$ bands are assumed to be midway between their $\Gamma_8$ and $\Gamma_7$ levels. For the present model, if $\delta_p$ and $\delta_d$ are made zero, the $E_1$, $E_0$, and $E_2$ levels, Eqs. (27) and (28), reduce to a doubly degenerate $\Gamma_8$ level at the energy $\lambda_1=\lambda_0$, and to a $\Gamma_7$ level at the energy $\lambda_2$, i.e.,

$$E_1=\lambda_1=E_0=\lambda_8(\Gamma_8),\quad E_2=\lambda_2(\Gamma_7)\ . \tag{43}$$

From Eqs. (36)—(38), it is seen that the fractional $p$-like characters then become

$$\alpha_1=\gamma_1=\alpha_0=\gamma_0\ ,\quad \alpha_2=\gamma_2\ . \tag{44}$$

The energy-gap anomaly $\Delta E_g$ [from Eq. (29)] becomes

$$\Delta E_g=E_1-\frac{\Delta_p}{3}=\lambda_1-\frac{\Delta_p}{3}\ . \tag{45}$$

Equations (43)—(45) are the same as those of Tell and Bridenbaugh, except for the different choice of the energy of the $\Gamma_{15}$ levels mentioned above.

### B. Kildal's model

In this case a noncubic crystal field is assumed, i.e., $\delta_p\neq0$ and $\delta_d\neq0$, but there is no $p$-$d$ hybridization, i.e., $M=0$. Thus, in the present analysis, if the $d$-like character is ignored, then only the $p$-like character remains and the various parameters take the values

$$\gamma_0=\gamma_1=\gamma_2=1,\quad \alpha_1=\alpha_0=\alpha_2=1 \tag{46}$$

and

$$\lambda_1=\lambda_0=\frac{\Delta_p}{3},\quad \lambda_2=-\tfrac{2}{3}\Delta_p\ .$$

The energies of the $\Gamma_7$ and $\Gamma_6$ levels can then be expressed as follows: For $\Gamma_6$,

$$E_0=\frac{\Delta_p+\delta_p}{3}\ , \tag{47}$$

and for $\Gamma_7$,

$$E_{1,2}=-\tfrac{1}{6}(\Delta_p+\delta_p)\pm\frac{1}{2}\left[\left[\Delta_p-\frac{\delta_p}{3}\right]^2+\tfrac{8}{9}\delta_p^2\right]^{1/2}\ . \tag{48}$$

This is identical to Kildal's final result. Furthermore, it is to be noted that Kane's form can be obtained by neglecting the crystal field completely, i.e., by setting $\delta_p=0$.

### C. Linear hybridization limit

This is the form used by various workers.[1,10,11,16] Essentially, it assumes that the parameters $\Delta$ and $\delta$ in Eq. (1) can each be written as a linear sum of the $p$ and $d$ contributions, i.e.,

$$\Delta=\alpha_L\Delta_p+(1-\alpha_L)\Delta_d$$

and

$$\delta=\alpha_L\delta_p+(1-\alpha_L)\delta_d\ . \tag{49}$$

In the present model, this case is represented by the conditions $M/E<1$ and $E>\Delta_p$ and $|\Delta_d|$. The energy eigenvalues $\lambda_1$ and $\lambda_2$ can then be rewritten, using a Taylor expansion, as

$$\lambda_1=\frac{1}{2}\left[\frac{\Delta_p}{3}-E-\frac{|\Delta_d|}{3}\right]+\frac{1}{2}\left[\frac{\Delta_p}{3}+E+\frac{|\Delta_d|}{3}\right]\left[1+\frac{4M^2}{(E+\Delta_p/3+|\Delta_d|/3)^2}\right]^{1/2}$$

$$\simeq\frac{\Delta_p}{3}+\frac{M^2}{E[1+(\Delta_p+|\Delta_d|)/3E]}\ . \tag{50}$$

Expanding further,

$$\lambda_1 \simeq \frac{M^2}{E} + \frac{\Delta_p}{3}\left[1-\frac{M^2}{E^2}\right] - \frac{M^2}{E^2}\frac{|\Delta_d|}{3} . \quad (51)$$

The first term on the right-hand side represents the shift due to hybridization and will be the same for all three bands. Hence it will disappear when the differences $E_1 - E_0$, etc. are calculated. However, it will be an important term in the expression for the band-gap anomaly $\Delta E_g$. Similarly,

$$\lambda_2 \simeq \frac{M^2}{E} - \frac{2\Delta_p}{3}\left[1-\frac{M^2}{E^2}\right] + \frac{2}{3}\frac{M^2}{E^2}|\Delta_d| . \quad (52)$$

Thus,

$$\lambda_1+\lambda_2 = \frac{2M^2}{E} - \frac{\Delta_p}{3}\left[1-\frac{M^2}{E^2}\right] + \frac{1}{3}\frac{M^2}{E^2}|\Delta_d| . \quad (53)$$

Similarly,

$$\lambda_1-\lambda_2 = \Delta_p\left[1-\frac{M^2}{E^2}\right] - |\Delta_d|\frac{M^2}{E^2} . \quad (54)$$

From Eqs. (18) and (19),

$$\gamma_1=\gamma_0=\gamma_2=\alpha_L \simeq \left[1-\frac{M^2}{E^2}\right] . \quad (55)$$

Thus,

$$\lambda_1+\lambda_2 = \frac{2M^2}{E} - \tfrac{1}{3}[\alpha_L\Delta_p - (1-\alpha_L)|\Delta_d|]$$

and

$$\lambda_1-\lambda_2 = \alpha_L\Delta_p - (1-\alpha_L)|\Delta_d| . \quad (56)$$

From Eq. (27),

$$E_0 = \lambda_0 + \gamma_0\delta_p/3 + (1-\gamma_0)\delta_d/3 ,$$

so that, in the linear hybridization limit,

$$E_0 \simeq \frac{M^2}{E} + \tfrac{1}{3}[\alpha_L\Delta_p - (1-\alpha_L)|\Delta_d|] + \tfrac{1}{3}[\alpha_L\delta_p + (1-\alpha_L)\delta_d] . \quad (57)$$

Similarly, from Eq. (28),

$$E_{1,2} = \frac{1}{2}\left[\lambda_1+\lambda_2-\gamma_1\frac{\delta_p}{3}-(1-\gamma_1)\frac{\delta_d}{3}\right] \pm \frac{1}{2}\left[\left[\lambda_1-\lambda_2-\gamma_1\frac{\delta_p}{3}-(1-\gamma_1)\frac{\delta_d}{3}\right]^2 + \tfrac{8}{9}\{(\gamma_1\gamma_2)^{1/2}\delta_p + [(1-\gamma_1)(1-\gamma_2)]^{1/2}\delta_d\}^2\right]^{1/2} ,$$

which, in the limit, gives

$$E_{1,2} \simeq \frac{M^2}{E} - \tfrac{1}{6}[\alpha_L\Delta_p - (1-\alpha_L)|\Delta_d| + \alpha_L\delta_p + (1-\alpha_L)\delta_d] \pm \tfrac{1}{2}(\{[\alpha_L\Delta_p - (1-\alpha_L)|\Delta_d|] - \tfrac{1}{3}[\alpha_L\delta_p + (1-\alpha_L)\delta_d]\}^2 + \tfrac{8}{9}[\alpha_L\delta_p + (1-\alpha_L)\delta_d]^2)^{1/2} . \quad (58)$$

The band-gap anomaly $\Delta E_g$ now becomes

$$\Delta E_g = E_1 - \frac{\Delta_p}{3} \simeq \frac{M^2}{E} - \frac{\Delta_p}{3} - \tfrac{1}{6}[\alpha_L\Delta_p - (1-\alpha_L)|\Delta_d| + \alpha_L\delta_p + (1-\alpha_L)\delta_d] + \tfrac{1}{2}(\{[\alpha_L\Delta_p - (1-\alpha_L)|\Delta_d|] - \tfrac{1}{3}[\alpha_L\delta_p + (1-\alpha_L)\delta_d]\}^2 + \tfrac{8}{9}[\alpha_L\delta_p + (1-\alpha_L)\delta_d]^2)^{1/2} . \quad (59)$$

In Eqs. (47) and (48), from the Kildal model, it can be assumed that $\Delta_p$ and $\delta_p$ are the total spin-orbit and crystal-field contributions, i.e., $\Delta_p$ is replaced by $\Delta$, and $\delta_p$ by $\delta$. If, in that modified form, $\Delta$ and $\delta$ are substituted from Eq. (49), the resulting equations are identical with Eqs. (57) and (58) above. Thus Eqs. (57)—(59) include the linear form assumed in previous work.[1,10,11,16]

## IV. NUMERICAL ANALYSIS AND RESULTS

In order to apply the present model to analyze the behavior of various I-III-$VI_2$ compounds, it is first necessary to review what experimental data are available for the analysis. For many of the I-III-$VI_2$ compounds, three valence-band—conduction-band transitions $E_A$, $E_B$, and $E_C$ have been determined at room temperature and are listed in Table I. The lattice-parameter values have been determined for all of the compounds, so that the ratio $c/a$ is known and is also given in Table I. However, if only these data were assumed known, there would be too many unknown parameters in the analysis. The band-gap anomaly $\Delta E_g$ can be estimated by comparing the value of $E_A$ with the value of the corresponding binary analog, and these values of $\Delta E_g$ are listed in Table I. Finally, values of the spin-orbit-splitting parameters $\Delta_p$ and $\Delta_d$ can be estimated from the atomic values.[12,13] Thus, $\Delta_p$ can be written in the form

$$\Delta_p = G_p(\tfrac{1}{16}\Delta_{p\,\mathrm{I}} + \tfrac{3}{16}\Delta_{p\,\mathrm{III}} + \tfrac{12}{16}\Delta_{p\,\mathrm{VI}}) , \quad (60)$$

where $\Delta_{p\,\mathrm{I}}$, etc. are the atomic $p$ spin-orbit splittings of the elements and $G_p$ is an enhancement factor for the

TABLE I. Input parameters.

| Code letter | Ternary compound | Energy gaps (eV) $E_A$ | $E_B$ | $E_C$ | $\Delta_p$ (eV) | $c/a$ | Binary analog[a] | Band-gap anomaly $\Delta E_g$ (eV) |
|---|---|---|---|---|---|---|---|---|
| *A* | $CuAlS_2$ | 3.49[b] | 3.62[b] | 3.62[b] | 0.09 | 1.96[b] | $Mg_{0.5}Zn_{0.5}S$ | 2.41[a] |
| *B* | $CuGaS_2$ | 2.43[b] | 2.55[b] | 2.55[b] | 0.12 | 1.96[b] | ZnS | 1.37[a] |
| *C* | $CuInS_2$ | 1.53[b] | 1.53[b] | 1.53[b] | 0.16 | 2.00[b] | $Zn_{0.5}Cd_{0.5}S$ | 1.64[a] |
| *D* | $CuAlSe_2$ | 2.72[c] | 2.86[c] | 3.01[c] | 0.32 | 1.95[b] | $Mg_{0.5}Zn_{0.5}Se$ | 1.47[a] |
| *E* | $CuGaSe_2$ | 1.68[b] | 1.75[b] | 1.96[b] | 0.35 | 1.96[b] | ZnSe | 1.00[a] |
| *F* | $CuInSe_2$ | 1.04[b] | 1.04[b] | 1.27[b] | 0.39 | 2.00[b] | $Zn_{0.5}Cd_{0.5}Se$ | 1.29[a] |
| *G* | $CuAlTe_2$ | 2.06[d] | | | 0.91 | 1.97[b] | $Mg_{0.5}Zn_{0.5}Te$ | 1.44[a] |
| *H* | $CuGaTe_2$ | 1.24[e] | 1.27[e] | 1.85[d] | 0.94 | 1.98[b] | ZnTe | 1.32[f] |
| *I* | $CuInTe_2$ | 1.06[e] | 1.06[e] | 1.67[e] | 0.98 | 2.00[b] | $Zn_{0.5}Cd_{0.5}Te$ | 1.12[f] |
| *J* | $AgAlS_2$ | 3.13[d] | | | 0.10 | 1.772[g] | $Mg_{0.5}Cd_{0.5}S$ | |
| *K* | $AgGaS_2$ | 2.73[b] | 3.01[b] | 3.01[b] | 0.13 | 1.79[b] | $Zn_{0.5}Cd_{0.5}S$ | 0.44[a] |
| *L* | $AgInS_2$ | 1.87[b] | 2.02[b] | 2.02[b] | 0.17 | 1.92[b] | CdS | 0.66[a] |
| *M* | $AgAlSe_2$ | 2.55[d] | | | 0.33 | 1.793[g] | $Mg_{0.5}Cd_{0.5}Se$ | |
| *N* | $AgGaSe_2$ | 1.83[b] | 2.03[b] | 2.29[b] | 0.354 | 1.82[b] | $Zn_{0.5}Cd_{0.5}Se$ | 0.50[a] |
| *O* | $AgInSe_2$ | 1.24[b] | 1.33[b] | 1.60[b] | 0.40 | 1.92[b] | CdSe | 0.61[a] |
| *P* | $AgAlTe_2$ | 2.27[h] | 2.38[h] | | 0.92 | 1.88[b] | $Mg_{0.5}Cd_{0.5}Te$ | 1.03[f] |
| *Q* | $AgGaTe_2$ | 1.32[i] | 1.43[i] | 2.23[i] | 0.95 | 1.90[b] | $Zn_{0.5}Cd_{0.5}Te$ | 0.86[f] |
| *R* | $AgInTe_2$ | 0.96[j] | | | 0.99 | 1.96[b] | CdTe | 0.84[f] |

[a]Reference 7.
[b]Reference 1.
[c]Reference 18.
[d]Reference 19.
[e]Reference 16.
[f]Reference 3.
[g]Reference 20.
[h]Reference 17.
[i]Reference 21.
[j]Reference 22.

solid. For both zinc-blende[12] and chalcopyrite[13] structures, $G_p$ has been taken to be 29/20. The values of $\Delta_{p\,\mathrm{I}}$, etc. used in the analysis have been taken from various sources and are listed in Table II. For $\Delta_d$, only the effects of the copper or silver *d* electrons are considered since the other *d* levels are much too deep to contribute. Thus $\Delta_d$ is assumed to be given by

$$\Delta_d = G_d \Delta_{d\,\mathrm{I}} . \tag{61}$$

Since, as indicated above, the *d* triplet acts like the *p* levels, it is assumed that $G_d$ also has the value 29/20. Taking $\Delta_{d\,\mathrm{Cu}}$ as $-0.152$ eV and $\Delta_{d\,\mathrm{Ag}}$ as $-0.55$ eV,[15] this gives $\Delta_d$ values of $-0.22$ eV for the copper compounds and $-0.80$ eV for the silver compounds.

The final requirement in this collection of input data is to obtain the crystal-field *p* splitting $\delta_p$ from the lattice-parameter ratio $c/a$. As indicated in Ref. 1, the relation can be written in the form

$$\delta_p = \tfrac{3}{2} b_p (2 - c/a) , \tag{62}$$

where $b_p$ is the deformation potential associated with the *p* character. Because of the interaction with the *d* bands, no explicit value for $b_p$ has been determined for the I-III-$VI_2$ compounds. However, for the II-IV-$V_2$ compounds, where no *p-d* hybridization occurs, the mean value of $b_p$ for the various compounds is found to be $-1.2$ eV. Thus this value was used initially for $b_p$ in the present work. However, as is shown below, a different value was needed in the final analysis.

With the above parameters taken as known, the number of unknowns in the analysis is reduced to three, viz., *E*, *M*, and $\delta_d$, and thus Eqs. (27)—(29) can be solved exactly to determine values for these parameters. From these values of *E*, *M*, and $\delta_d$, values can be determined for $E_1$, $E_0$, $E_2$, $\alpha_1$, $\alpha_0$, and $\alpha_2$ from Eqs. (27), (28), and (36)—(42). The differences between the $E_1$, $E_0$, and $E_2$ values should, of course, be the same as the differences between the $E_A$, $E_B$, and $E_C$ input values, but the separate values will be different by a constant quantity since the energy zero in the present analysis was chosen to be at the $\Gamma_{15}$ level of the initial quasicubic crystal, as is shown in Fig. 1.

TABLE II. Atomic *p* spin-orbit splittings of elements used in the analysis (in eV).

| | | |
|---|---|---|
| $\Delta_p$(Cu)=0.031[a] | $\Delta_p$(Ga)=0.12[b] | $\Delta_p$(S)=0.077[c] |
| | $\Delta_p$(Al)=0.016[b] | $\Delta_p$(Se)=0.286[c] |
| $\Delta_p$(Ag)=0.114[a] | $\Delta_p$(In)=0.27[b] | $\Delta_p$(Te)=0.8335[c] |

[a]References 14 and 15.
[b]Reference 12.
[c]Reference 13.

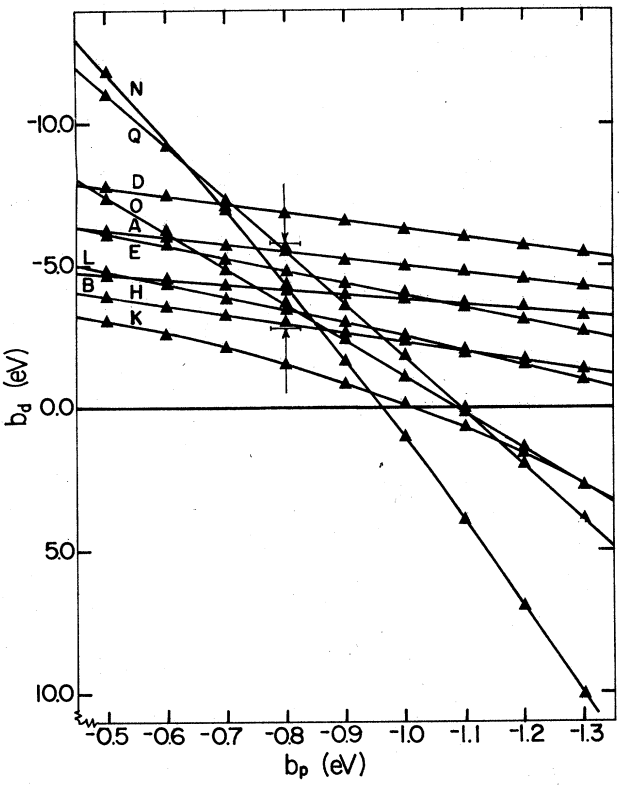


FIG. 2. Values of $b_d$ obtained in present analysis for given values of $b_p$. For meaning of code letters, see Table I. $\perp\!\!\!\top$ denotes the mean $b_d \pm \sigma$ at $b_p = -0.8$ eV.

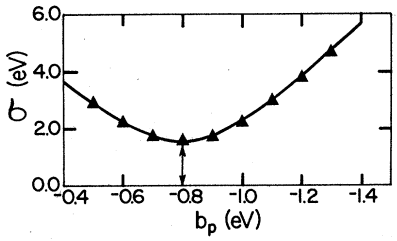


FIG. 3. Variation of standard deviation $\sigma$ for $b_d$ (averaged over 13 compounds) for given values of $b_p$.

The values of $\alpha_1$, $\alpha_0$, and $\alpha_2$ show the relative amount of $p$ character in the three separate valence bands. In each case the variation from one band to another is quite small, but it is of interest for purposes of comparison to have $\bar{\alpha}$ as a mean value, i.e., $\bar{\alpha} = \frac{1}{3}(\alpha_1 + \alpha_0 + \alpha_2)$.

When the above calculations were made using the value of $b_p = -1.2$ eV, it was found that the values obtained for the various parameters listed above appeared to be in satisfactory agreement from one compound to another, except in the case of $\delta_d$. On the assumption that $\delta_d$ satisfies the same form as $\delta_p$ with regard to the parameter ratio $c/a$, i.e.,

$$\delta_d = \tfrac{3}{2} b_d (2 - c/a) ,$$

it was possible to obtain values of $b_d$ for all compounds considered. These were found to vary considerably, with

TABLE III. Parameters determined from the analysis.

| Ternary compound | $E_1$ (eV) | $E_0$ (eV) | $E_2$ (eV) | $\alpha_1$ | $\alpha_0$ | $\alpha_2$ | $\bar{\alpha}$ |
|---|---|---|---|---|---|---|---|
| $CuAlS_2$ | 2.44 | 2.31 | 2.31 | 0.707 | 0.713 | 0.702 | 0.707 |
| $CuGaS_2$ | 1.41 | 1.29 | 1.29 | 0.645 | 0.660 | 0.632 | 0.646 |
| $CuInS_2$ | 1.69 | 1.69 | 1.69 | 0.602 | 0.602 | 0.556 | 0.587 |
| $CuAlSe_2$ | 1.57 | 1.43 | 1.28 | 0.746 | 0.750 | 0.715 | 0.737 |
| $CuGaSe_2$ | 1.12 | 1.05 | 0.84 | 0.812 | 0.813 | 0.777 | 0.801 |
| $CuInSe_2$ | 1.42 | 1.42 | 1.19 | 0.760 | 0.760 | 0.715 | 0.745 |
| $CuAlTe_2$ | | | | | | | |
| $CuGaTe_2$ | 1.63 | 1.60 | 1.02 | 0.752 | 0.752 | 0.656 | 0.720 |
| $CuInTe_2$ | 1.45 | 1.45 | 0.84 | 0.749 | 0.749 | 0.628 | 0.709 |
| $AgAlS_2$ | | | | | | | |
| $AgGaS_2$ | 0.483 | 0.203 | 0.203 | 0.864 | 0.901 | 0.830 | 0.865 |
| $AgInS_2$ | 0.717 | 0.567 | 0.567 | 0.824 | 0.855 | 0.802 | 0.827 |
| $AgAlSe_2$ | | | | | | | |
| $AgGaSe_2$ | 0.618 | 0.418 | 0.158 | 0.965 | 0.966 | 0.958 | 0.963 |
| $AgInSe_2$ | 0.743 | 0.653 | 0.383 | 0.928 | 0.929 | 0.904 | 0.920 |
| $AgAlTe_2$ | | | | | | | |
| $AgGaTe_2$ | 1.17 | 1.06 | 0.26 | 0.948 | 0.948 | 0.935 | 0.944 |
| $AgInTe_2$ | | | | | | | |

TABLE IV. Parameters determined from the analysis.

| Ternary compound | $M$ (eV) | $E$ (eV) | $M/E$ | $1-\bar{\alpha}$ | $\Delta E_g/E$ | $1-\alpha_1$ | $1-\alpha^a$ | $1-\alpha_L$ |
|---|---|---|---|---|---|---|---|---|
| $CuAlS_2$ | 3.660 | 3.340 | 1.096 | 0.293 | 0.722 | 0.293 | 0.352 | 0.290 |
| $CuGaS_2$ | 1.794 | 1.096 | 1.637 | 0.354 | 1.250 | 0.355 | 0.315 | 0.353 |
| $CuInS_2$ | 2.015 | 0.708 | 2.846 | 0.413 | 2.316 | 0.398 | 0.240 | 0.421 |
| $CuAlSe_2$ | 2.396 | 2.588 | 0.926 | 0.263 | 0.568 | 0.254 | 0.275 | 0.254 |
| $CuGaSe_2$ | 2.006 | 3.037 | 0.661 | 0.199 | 0.329 | 0.188 | 0.251 | 0.203 |
| $CuInSe_2$ | 2.294 | 2.585 | 0.887 | 0.255 | 0.499 | 0.240 | 0.220 | 0.262 |
| $CuAlTe_2$ | | | | | | | | |
| $CuGaTe_2$ | 2.275 | 2.271 | 1.002 | 0.280 | 0.581 | 0.248 | | 0.298 |
| $CuInTe_2$ | 1.935 | 1.822 | 1.062 | 0.291 | 0.615 | 0.251 | | 0.308 |
| $AgAlS_2$ | | | | | | | | |
| $AgGaS_2$ | 0.757 | 1.716 | 0.441 | 0.135 | 0.256 | 0.136 | | 0.140 |
| $AgInS_2$ | 1.352 | 2.396 | 0.564 | 0.173 | 0.275 | 0.176 | | 0.175 |
| $AgAlSe_2$ | | | | | | | | |
| $AgGaSe_2$ | 2.028 | 9.962 | 0.204 | 0.037 | 0.050 | 0.035 | | 0.037 |
| $AgInSe_2$ | 2.020 | 6.323 | 0.319 | 0.080 | 0.096 | 0.072 | | 0.082 |
| $AgAlTe_2$ | | | | | | | | |
| $AgGaTe_2$ | 3.432 | 13.30 | 0.258 | 0.056 | 0.065 | 0.052 | | 0.059 |
| $AgInTe_2$ | | | | | | | | |

[a]Reference 7.

values from $-5.8$ to $+6.9$ eV. Since it had further been assumed that, as in the case of $b_p$, $b_d$ should have the same value for all of those compounds, the above result was taken to indicate that the value assumed for $b_p$ was incorrect. The complete analysis was therefore repeated a number of times using values of $b_p$ lying in the range $-0.5$ to $-1.8$ eV and the values obtained for $b_d$ compared in each case. Figure 2 shows the values of $b_d$ obtained for each compound for values of $b_p$ in the range $-0.5$ to $-1.3$ eV. It is apparent that the spread in $b_d$ values appears smallest for $b_p$ in the vicinity of $-0.8$ eV. For each value of $b_p$, a mean value of $b_d$ and a standard deviation $\sigma$ were calculated. Figure 3 shows the variation of $\sigma$ with $b_p$. It is seen that the minimum in $\sigma$ occurs at $b_p=-0.8$ eV, at which point the mean value of $b_d$ is $-4.3$ eV and $\sigma=1.5$ eV. In view of these results, it is suggested that for all of the I-III-$VI_2$ compounds and alloys, appropriate values for the deformation potentials are $b_p=(-0.8\pm0.2)$ eV and $b_d=(-4.3\pm1.5)$ eV.

Unlike $b_d$, the other parameters determined by the analysis were found to be relatively insensitive to variations in $b_p$. Thus, in the final calculations the method described above was used with a value of $b_p=-0.8$ eV. The resulting values of the parameters $E$, $M$, $E_1$, $E_0$, $E_2$, $\alpha_1$, $\alpha_0$, $\alpha_2$, and $\bar{\alpha}$ are listed in Tables III and IV. Also given in these tables for purposes of comparison are values of $1-\alpha_L$ given by various authors from linear-hybridization-type models.

The ratios $M/E$ and $\Delta E_g/E$ are dimensionless and indicate the general character of the model. These ratios are

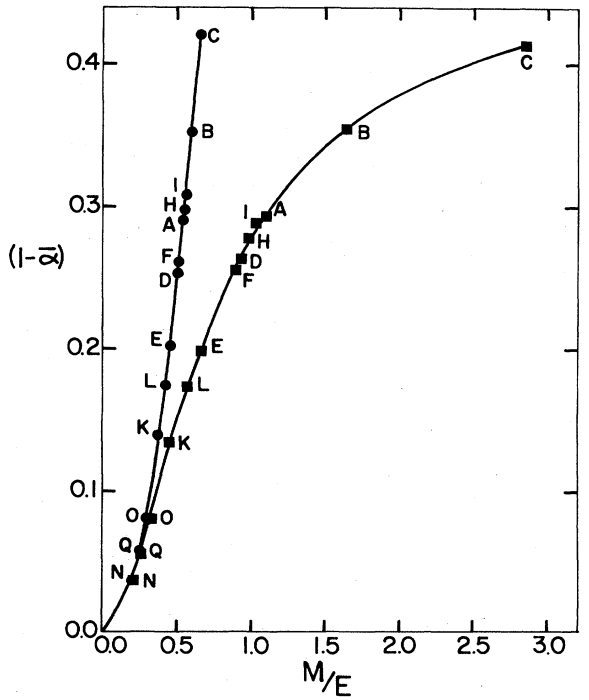


FIG. 4. Variation of mean value of fractional $d$ character of valence band $1-\bar{\alpha}$ with $M/E$. ■, present model; ●, linear hybridization approximation. For meaning of code letters, see Table I.

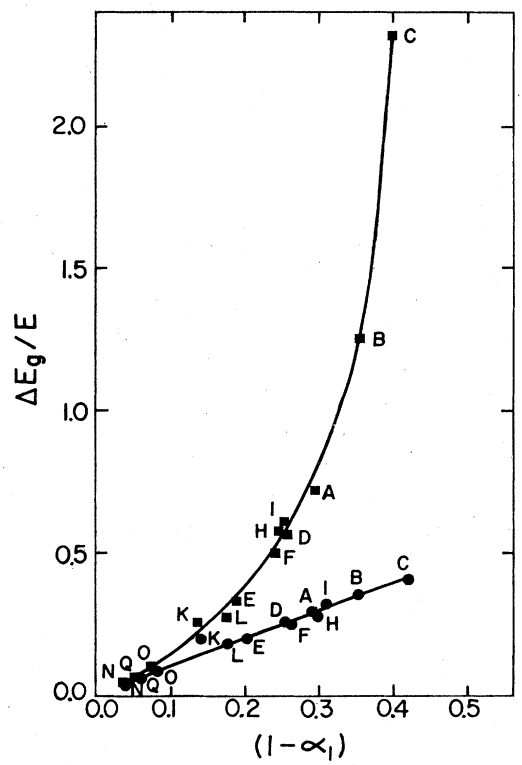


FIG. 5. Variation of $\Delta E_g/E$ with fractional $d$ character of top valence band $1-\alpha_1$. ■, present model; ●, linear hybridization approximation. For meaning of code letters, see Table I.

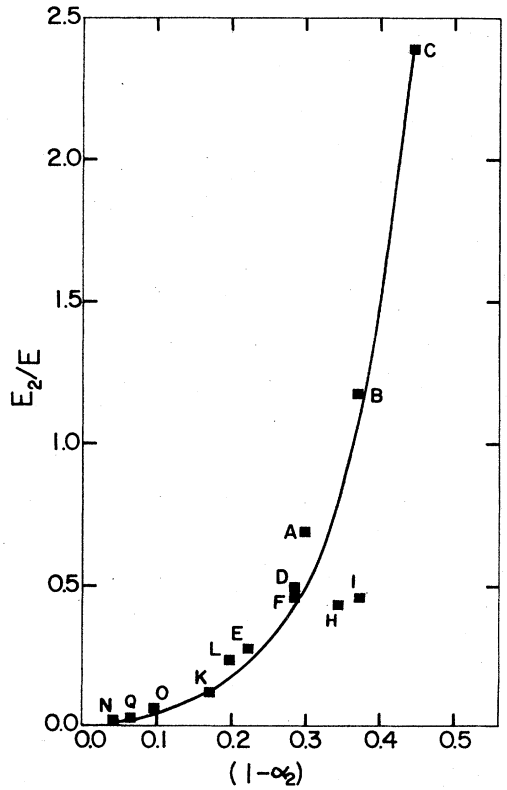


FIG. 6. Variation of $E_2/E$ with fractional $d$ character $(1-\alpha_2)$. For meaning of code letters, see Table I.

given in Table IV. Figure 4 shows the values of $1-\bar{\alpha}$, i.e., the mean fraction of $d$ character in the three bands, plotted against $M/E$ while Fig. 5 gives the values of $\Delta E_g/E$ plotted against $1-\alpha_1$, the fraction of $d$ character in the top valence band. It is seen that the values for the different compounds lie on smooth curves which appear to be characteristic of the structure. In Figs. 4 and 5, values determined from the linear hybridization model are also given for comparison. These curves will be discussed further below.

Finally, the variation of the reduced energy values $E_1/E$, $E_0/E$, and $E_2/E$ should depend, respectively, on the values of $\alpha_1$, $\alpha_0$, and $\alpha_2$. In Fig. 6 the variation of $E_2/E$ with $1-\alpha_2$ is given, and the variation of the other parameters is very similar to this.

## V. DISCUSSION

The aim of the work has been to produce a theoretical model describing the effect of $p$-$d$ hybridization in the valence band of a I-III-$VI_2$ compound, the starting point being the Kane model[6] for a binary compound with spin-orbit interaction. Since the states of the triple part of the $d$ band have the same symmetry as those of the $p$ band, it has been assumed that their matrix representations have the same form. Thus when $p$-$d$ hybridization is applied, the $p$ and $d$ bands mix and repel each other. In the present analysis the magnitude of this mixing and repulsion can be calculated exactly. After this, the crystal-field interaction is introduced and again the calculation can be performed exactly.

A number of points should be mentioned here. Firstly, the order of the operations with the crystal-field effect applied last is different from that used by Kildal. However, since each step is carried out exactly, the order of application should not affect the final result. The order used here was found to simplify the mathematics. Secondly, in order to reduce the number of unknown parameters in the analysis, the off-diagonal matrix elements due to crystal-field interaction between the $p$ and $d$ bands have been neglected, i.e., it has been assumed that

$$\langle X \mid V_{\rm cr} \mid YZ \rangle = \langle Y \mid V_{\rm cr} \mid ZX \rangle = \langle Z \mid V_{\rm cr} \mid XY \rangle = 0 \, .$$

Since $M$ and $E$ are used as adjustable parameters, this means that the effect of this interband interaction will be taken up in the values determined for $M$ and $E$. Finally, in the crystal-field analysis the effect of the anion displacement, the structure component discussed by Jaffe and Zunger, has been neglected, since this would require a much more detailed analysis involving atomic positions, etc. It is considered that this structural component has an appreciably smaller effect than that of the tetragonal distortion given by $2-c/a$.

In order to use the model to analyze the experimental data for various compounds, in addition to the measured values of $E_A$, $E_B$, and $E_C$, the valence-band—conduction-band transition energies, and also of $c/a$, the lattice-parameter ratio, it is necessary to know $\Delta_p$ and $\Delta_d$, which here are calculated from atom spin-orbit values, and also one other parameter. In the present analysis, $\Delta E_g$, the band-gap anomaly, has been used. This can be

determined for most of the compounds considered by subtracting the value of $E_A$ from the energy-gap value of the equivalent binary compound, either real, e.g., ZnS, etc., or a pseudocompound, e.g., $Mg_{0.5}Zn_{0.5}S$, etc. This involves a further assumption in the theoretical analysis that $\Delta E_g$ can be equated to the energy separation of the $E_1(\Gamma_7)$ and $\Gamma_8(p)$ level in Fig. 1, an assumption made previously by Tell and Bridenbaugh. The analysis then enables the mean values of the deformation potentials $b_p$ and $b_d$ to be determined over the range of compounds considered. This is an important point for analysis of further materials since, now, the extra parameter assumed known can be $b_d$ rather than $\Delta E_g$. It is planned to extend this analysis to the temperature variation of the energy gaps of a number of the compounds, and also to the variation of energy gaps with both composition and temperature for a number of alloys of the compounds. In none of these cases will the value of $\Delta E_g$ be available; thus acceptable values of the deformation potentials are essential.

As indicated above, $M/E$ and $\Delta E_g/E$ are dimensionless and the former determines the fractional $d$ character in the valence band $(1-\bar{\alpha})$. Hence, Figs. 4 and 5 show plots of $1-\bar{\alpha}$ versus $M/E$ and $\Delta E_g/E$ versus $1-\alpha_1$ for all compounds considered. In each, all of the points lie on a single smooth curve, indicating that $M/E$ and $\Delta E_g/E$ are characteristic of the structure. Also plotted in the figures are the values determined from the linear hybridization approximation. These graphs clearly indicate where the linear model breaks down. Thus for the case of $1-\bar{\alpha}$ versus $M/E$, the linear model indicates that all values of $1-\bar{\alpha}$ up to the maximum of 1 could be obtained with relative small values of $M/E$, even in the case when an initial postulate was that the $p$ levels were higher than the $d$ levels. However, the present model indicates that $1-\bar{\alpha}$ is limited to approximately 0.5, whatever values of $M/E$ are considered. Similarly, in the case of $\Delta E_g/E$ versus $1-\alpha_1$, the linear model indicates a maximum value for $\Delta E_g/E$ of approximately 1, even with values of $1-\alpha_1$ up to 1, while the present model allows very much larger values of $\Delta E_g/E$, although $1-\alpha_1$ is limited to a maximum of approximately 0.5. This comment is similar to that made by Jaffe and Zunger concerning the plot of $\Delta E_g$ versus $1-\alpha_L$ by Shay and Kasper. The latter was assumed to give a linear variation and fitted fairly well for low $\Delta E_g$ values. However, in the case of $CuAlS_2$, the value of $\Delta E_g$ of 2.4 eV would indicate a value for $1-\alpha_L$ of 0.77, very different from the value of 0.35 determined from the spin-orbit splitting. It is to be noted that Shay and Kasper made the CuCl value a point on their line. If this had been ignored and the $CuAlS_2$ value used, a curve similar in shape to that of Fig. 4 would have been obtained.

In Table IV values of $1-\bar{\alpha}$ from the present analysis are given together with values of $1-\alpha$ from Jaffe and Zunger and Shay and Wernick. The values show appreciable differences in some cases, and this could be due to the methods of analysis. Thus, in the theoretical calculations of Jaffe and Zunger, spin-orbit splitting was neglected, while in the present calculations the structural component of the crystal-field effect was neglected. In the Shay and Wernick results, the values of $\Delta_p$ used were taken from the binary analogs and not from the atomic values, as in the present work.

For the I-III-$VI_2$ chalcopyrite compounds, the experimental evidence indicates that the three valence bands have $\Gamma_7\Gamma_6\Gamma_7$ symmetry in order of energy values. However, the experimental results for $CuGa(S_zSe_{1-z})_2$ have been interpreted by Tell and Bridenbaugh[9] to indicate that the $\Gamma_6$ and $\Gamma_7$ bands cross over at $z$ of the order of 0.95 so that the $CuGaS_2$ order would $\Gamma_7\Gamma_7\Gamma_6$. However, in this case they found it necessary to postulate that the $d$ levels lay above the $p$ levels in the starting model. It is possible to explain these results with the present model. For all of the sulfides, $\Delta_p$, the $p$ spin-orbit splitting, is small, and, as seen from Fig. 1, the effect of $p$-$d$ hybridization further reduces the $\Gamma_8-\Gamma_7$ difference, and hence the $E_0-E_2$ difference, after the effect of the crystal field is included. There is no limit, in this case, to the reduction, and $\Gamma_8-\Gamma_7$ (and hence $E_0-E_2$) could become zero or even change sign, depending upon the amount of hybridization (and the strength of the crystal-field interaction) occurring. Thus the $\Gamma_7\Gamma_7\Gamma_6$ order suggested for $CuGaS_2$ could occur, even though in the starting quasicubic structure the $d$ levels are well below the $p$ levels.

*Note added in proof.* The above analysis was carried out using the value $\Delta_{d\,Ag}=-0.55$ eV[15]. However, Cardona[14] gives a lower value to this parameter, namely $-0.33$ eV. Therefore the calculations have been redone using this lower value. It is found that in Fig. 2, although the curves corresponding to the silver compounds are changed to some extent, the region of minimum spread remains almost the same as before. This in this case the values obtained are $b_p=(-0.8\pm0.2)$ eV and $b_d=(-3.9\pm1.5)$ eV. In addition, in Figs. 4–6 the positions of the points for the silver compounds are changed by various amounts, but in all cases the points still lie on the curves shown. Thus the conclusions drawn are not affected.

## ACKNOWLEDGMENTS

The authors wish to acknowledge the invaluable contributions of the Canadian International Development Agency for financial support under the Institutional Link in Semiconductors between the Physics Department of Chulalongkorn University and the University of Ottawa. Two of them (K.Y.) and (V.S.) would like to thank Chulalongkorn University for financial support through the "UNIT CELL" program. The authors have benefited from discussions with Dr. K. S. Song and Dr. B. Joos.

*On leave from Chulalongkorn University, Bangkok 10500, Thailand.

[1]J. L. Shay and J. H. Wernick, *Ternary Chalcopyrite Semiconductors: Growth, Electronic Properties, and Applications* (Pergamon, Oxford, 1974).

[2]*Ternary Compounds, 1977,* edited by G. D. Holah (IOP Conference Series No. 35) (Institute of Physics, London, 1977).

[3]A. Miller, A. MacKinnon, and D. Weaire, in *Solid State Physics,* edited by H. Ehrenreich, F. Seitz, and D. Turnbull

(Academic, New York, 1981), Vol. 36, p. 119.
[4]J. J. Hopfield, J. Phys. Chem. Solids **15**, 97 (1960).
[5]H. Kildal, Phys. Rev. B **10**, 5082 (1974).
[6]E. O. Kane, J. Phys. Chem. Solids **1**, 249 (1957).
[7]J. E. Jaffe and A. Zunger, Phys. Rev. B **29**, 1882 (1984).
[8]M. J. Lucino and C. J. Vesely, Appl. Phys. Lett. **23**, 60 (1973), **23**, 453 (1973); S. Kono and M. Okusawa, J. Phys. Soc. Jpn. **37**, 1301 (1974).
[9]B. Tell and P. M. Bridenbaugh, Phys. Rev. B **12**, 3330 (1975).
[10]N. Yamamoto, H. Horinaka, K. Okada, and T. Miyauchi, Jpn. J. Appl. Phys. **16**, 1817 (1977).
[11]N. Yamamoto, H. Horinaka, and T. Miyauchi, Jpn. J. Appl. Phys. **18**, 255 (1979).
[12]R. Braunstein and E. O. Kane, J. Phys. Chem. Solids **23**, 1423 (1962).
[13]A. S. Poplavnoi and Yu. I. Polygalov, Izv. Akad. Nauk SSSR, Neorg. Mater. **7**, 1706 (1971); **7**, 1711 (1971) [Inorg. Mater. (USSR) **7**, 1527 (1971); **7**, 1531 (1971)].
[14]M. Cardona, *Modulation Spectroscopy* (Academic, New York, 1969), p. 67.
[15]Y. Yafet, in *Solid State Physics,* edited by F. Seitz and D. Turnbull (Academic, New York, 1963), Vol. 14, p. 1.
[16]M. J. Thwaites, R. D. Tomlinson, and M. J. Hampshire, in *Ternary Compounds 1977,* Ref. 2, p. 237.
[17]B. Tell, J. L. Shay, and M. Kasper, Phys. Rev. B **9**, 5203 (1974).
[18]M. Bettini, Solid State Commun. **13**, 599 (1973).
[19]W. N. Honeyman and K. H. Wilkinson, J. Phys. D **4**, 1182 (1971).
[20]H. W. Spiess, V. Haeberln, G. Brandt, A. Rauber, and J. Schneider, Phys. Status Solidi B **62**, 183 (1974).
[21]B. Sermage, F. Barthe-Lefin, and A. C. Papadopoulo-Scherle, J. Phys. (Paris) Colloq. **3**, C-137 (1975).
[22]B. R. Pamplin, T. Kiyosawa, and K. Masumoto, Prog. Cryst. Growth Charact. **1**, 331 (1979).